Structure and optical properties of high light output halide scintillators

David J. Singh

Materials Science and Technology Division and Center for Radiation Detection Materials and Systems,
Oak Ridge National Laboratory, Oak Ridge, Tennessee 37831-6114, USA
(Received 12 August 2010; revised manuscript received 13 October 2010; published 29 October 2010)

Structural and optical properties of several high light output halide scintillators and closely related materials are presented based on first-principles calculations. The optical properties are based on the Engel-Vosko generalized gradient approximation and the recently developed density functional of Tran and Blaha. The materials investigated are $BaBr_2$, $BaIBr$, $BaCl_2$, BaF_2, BaI_2, BiI_3, CaI_2, Cs_2LiYCl_6, $CsBa_2Br_5$, $CsBa_2I_5$, K_2LaBr_5, K_2LaCl_5, K_2LaI_5, $LaBr_3$, $LaCl_3$, $SrBr_2$, and YI_3. For comparison results are presented for the oxide $CdWO_4$. We find that the Tran Blaha functional gives greatly improved band gaps and optical properties in this class of materials. Furthermore, we find that unlike $CdWO_4$, most of these halides are highly isotropic from an optical point of view even though in many cases the crystal structures and other properties are not. This general result is rationalized in terms of halide chemistry. Implications for the development of ceramic halide scintillators are discussed.

I. INTRODUCTION

Scintillators are widely used in radiation detection applications including medical imaging, oil well drilling, nuclear security, and high-energy physics experiments. These materials function by emitting light when excited by ionizing radiation, such as gamma rays. This light is then coupled to a photomultiplier or other light detector to produce electrical signals. The performance of scintillators is characterized by their light output, normally given in terms of photons per megaelectron volt of excitation energy, proportionality (how linear the light output is as a function of excitation energy), density (related to stopping power), decay time, and energy resolution.[1]

Scintillator performance depends on energy transport between the energy absorption events and the scintillation centers, suppression of nonradiative recombination channels and fast efficient light emission from the scintillation center. These scintillation centers can be intrinsic, via a mechanism such as decay of a self-trapped exciton, or, as is commonly the case, at an activation center (e.g., Ce^{3+} ions substituting for La^{3+} in $LaBr_3$) where electron-hole pairs generated by the radiation recombine. These processes are sensitive to the details of the material and in the case of materials with activators the environment of the activator ions. Halides generally have soft lattices that disfavor nonradiative recombination and can typically incorporate rare earth and other activator ions. More importantly, halide chemistry is very rich with a wide variety of crystal structures that provide different bonding topologies for energy transfer and various environments for activator ions.[2,3] In fact, one of the best known scintillators is the halide, NaI activated with Tl^+. This material has high light output, but is slow, nonproportional and has poor energy resolution.[4] The finding that Ce^{3+} activated $LaBr_3$ is a very high light output proportional scintillator with energy resolution better than 3% at 662 KeV (Ref. 5) has led to renewed interest in halides as scintillator hosts, especially for spectroscopic gamma ray detection. This interest has resulted in the discovery of several other interesting halide scintilla-

tors, including heavily Eu^2-activated SrI_2, which is very proportional and has a light output exceeding that of $LaBr_3$,[6] and Ce^{3+}-activated YI_3, which is another very high light output material.[7]

Full characterization of the optical properties of scintillators is very useful both from the point of view of improving the design of systems as regards light coupling and also importantly in selecting candidate materials for ceramic scintillators. However, full optical characterization of these halides is complicated by sensitivity to moisture and other experimental difficulties. As a result only limited data is available.

The key requirements for a ceramic scintillator are sinterability and optical isotropy. This latter requirement comes from the need to avoid light scattering at misoriented grain boundaries. It is commonly thought that because of this requirement cubic material is needed for a true transparent ceramic. However, radiation detection is not an optical imaging application. Therefore weak scattering and image distortion are not as detrimental as they would be in an optical application such as a ceramic lens. In fact ceramic scintillators based on monoclinic Lu_2SiO_5 have been demonstrated.[8,9] We showed in previous work that the high light output halide scintillator, SrI_2 is in fact very nearly optically isotropic in spite of its orthorhombic (*Pbca*) crystal structure.[10] This was an unexpected result considering the strongly orthorhombic lattice. It is of interest to determine whether this is the case for other high light output halide scintillators. Here we present a consistent set of first-principles data for structural and optical properties of a number of high light output halide scintillators and closely related materials. We find, quite unexpectedly, that the halides we investigate have remarkably little optical anisotropy, even though a number of them are very anisotropic from other points of view.

II. APPROACH

The density-functional calculations reported here were performed using the general potential linearized augmented plane-wave (LAPW) method as implemented in the WIEN2K

code.[11] We used well-converged Brillouin-zone samples and basis sets, with the standard LAPW augmentation plus local orbitals.[12] Relativity was included at the scalar-relativistic level except for BiI$_3$, where spin orbit was included for the electronic structure.

The crystal structure plays a fundamental role in determining the electronic and optical properties of a material. We began our calculations by fully relaxing all free internal atomic positions consistent with the crystal symmetry for each material. The lattice parameters were held fixed at their experimental values, which are no doubt more precise than the values that can be obtained using density-functional calculations. This relaxation was done using the generalized gradient approximation (GGA) of Perdew, Burke, and Ernzerhof (PBE).[13]

The PBE functional, like other standard generalized gradient approximations, is based on the total energy in terms of the coupling constant averaged exchange correlation hole and is designed to reproduce the total energy.[14] While these functionals are very useful in obtaining structures and other properties related to total energies, they underestimate, often strongly, the band gaps of most semiconductors and simple insulators. Accordingly, for the optical properties we use two other functionals. The first is the Engel-Vosko (EV) GGA.[15] This functional was designed to reproduce the exact exchange potential rather than the total energy and gives improved band gaps.[16] We used it in our prior studies on transport in PbTe and optical properties of SrI$_2$ and Bi$_4$Ge$_3$O$_{12}$ scintillators.[10,17,18] Here we employ this functional with the GGA correlation potential of Perdew $et\ al.$[14] The second is the semilocal functional of Tran and Blaha (TB-mBJ).[19] This relatively recent functional is more sophisticated than the Engel-Vosko GGA and has been shown to give very much improved band gaps for a variety of semiconductors and insulators. We find that where comparison with experiment is possible this functional also gives very much improved band gaps as well as optical properties for these halides. As such, we focus on the results obtained using the TB-mBJ functional. The electronic structures were calculated with these two functionals based on the relaxed crystal structures from the PBE calculations. Optical properties were then obtained using the dipole matrix elements with the WIEN2K optical package.[11] A 0.1 eV broadening was applied to the spectra.

III. MATERIALS AND STRUCTURES

We begin with the calculated structural parameters and brief introductions to the materials that we study. BaF$_2$ is a very well-characterized material. It has been applied as a scintillator, both in pure form and with activation.[20–24] In pure form it has a very fast component ($\sim$0.8 ns), as well as a slow component, which can be at least partially suppressed by La doping. Fast response is of importance in applications with very high count rates or where timing is critical. It occurs in the cubic ($Fm\bar{3}m$) CaF$_2$ structure, Ba on Wyckoff site $4a$ (0,0,0) and F on $8c$ (1/4,1/4,1/4). In our calculations we used the experimental lattice parameter,[25] a=6.2001 Å.

Several of the alkaline earth dihalides, AeX_2, are high light output proportional scintillators when activated with

TABLE I. Structural properties of orthorhombic $Pnma$ PbCl$_2$ type, BaCl$_2$, BaBr$_2$, BaI$_2$, and BaIBr. The lattice parameters are from experiment (Refs. 33–35) while the internal parameters are from total-energy minimization using the PBE functional. For BaIBr, $X1$ is I and $X2$ is Br. All atoms are on Wyckoff site $4c$ with y=0.25.

	BaCl$_2$	BaBr$_2$	BaI$_2$	BaIBr
a (Å)	7.878	8.276	8.922	8.6
b (Å)	4.731	4.956	5.304	5.12
c (Å)	9.415	9.919	10.695	10.31
Ba x	0.2481	0.2470	0.2466	0.2302
Ba z	0.3838	0.1163	0.1166	0.1228
$X1$ x	0.1423	0.6426	0.6424	0.9722
$X1$ z	0.0708	0.0714	0.0721	0.6701
$X2$ x	0.5274	0.5266	0.5246	0.3538
$X2$ z	0.8313	0.6686	0.6665	0.4325

Eu^{2+}.[6,26–29] As with BaF$_2$, activation with Ce^{3+} is also possible in some cases.[30] Undoped BaCl$_2$ has a very fast response, with a short component lifetime of 1.6 ns.[31] SrI$_2$:Eu is equal to or superior to LaBr$_3$:Ce^{3+} as regards light output and proportionality, although it suffers from a slower response.[6] Even though the material is orthorhombic, we found it to be optically nearly isotropic.[10] CaI$_2$:Eu^{2+} is another material with very high light output, $\sim$100 000 photons/MeV.[6,27] BaIBr:Eu^{2+} crystals have been shown to have a light output of 81 000 ± 3000 photons/MeV with a 662 KeV energy resolution better than 5%.[32] Regarding structure, BaCl$_2$, BaBr$_2$, BaI$_2$, and BaIBr occur in an orthorhombic $Pnma$, PbCl$_2$-type structure with 4 f.u./cell. The structural parameters as determined from relaxation are given in Table I. SrBr$_2$ has a large tetragonal unit cell ($P4/nz$) with 10 f.u./cell.[36] The calculated internal parameters are as given in Table II. CaI$_2$ is hexagonal ($P\bar{3}m1$) with Ca on site $1a$ (0,0,0) and I on $2d$(1/2,2/3,z). In our optical calculations we used the experimental lattice parameters, a=4.49 Å, c=6.975 Å, with the calculated z=0.2535 from total-energy minimization with the PBE GGA (the reported experimental value is 0.25).[37]

LaCl$_3$ and LaBr$_3$ activated with Ce^{3+} are very high light output, proportional scintillators with excellent energy resolution.[5] They are hexagonal ($P6_3/m$) with the UCl$_3$ structure type. There are 2 f.u./cell, with La on site $2c$ (1/3,2/3,1/4) and the halogen on $6h(u,v,1/4)$. We used the experimental lattice parameters, a=7.4779 Å, c=4.3745 Å, for LaCl$_3$ (Ref. 38) and a=7.9648 Å, c=4.5119 Å, for LaBr$_3$ (Ref. 39). The calculated internal parameters were u=0.9145, v=0.6132 for LaCl$_3$ and u=0.9144, v=0.6159 for LaBr$_3$.

Cs$_2$LiYCl$_6$ is a member of the elpasolite family. The elpasolites are cubic $Fm\bar{3}m$ halides, with general formula $A1_2A2RX_6$, with $A1$ and $A2$ alkali metals, X a halogen, and R a rare earth or other trivalent element. $A1$ is on site $8c$ (1/4,1/4,1/4), $A2$ is on $4b$ (1/2,1/2,1/2), R is on $4a$ (0,0,0) and X is on $24e(u,0,0)$. A large number of such compounds are known.[3] However, only a fraction have been studied as po-

TABLE II. Internal structural coordinates of tetragonal $P4/nz$ (No. 85) $SrBr_2$ as determined by total-energy minimization. The lattice parameters were fixed at their experimental values of $a=11.630$ Å and $c=7.146$ Å (Ref. 36).

	Sr1	Sr2	Br1	Br2	Br3	Br4
x	0.4141	0.7500	0.5402	0.5426	0.2500	0.2500
y	0.6035	0.7500	0.6527	0.8386	0.7500	0.7500
z	0.7520	0.1487	0.3761	0.9004	0.0000	0.5000

tential scintillator materials.[40–46] Cs_2LiYCl_6 is of particular interest because of its high Li content, which makes it useful as a neutron detector. We used the experimental lattice parameter for Cs_2LiYCl_6 from Reber *et al.*,[47] $a=10.4857$ Å, with the calculated internal parameter $u=0.2517$ (an experimental value of 0.25046 was reported by Reber and coworkers).

The scintillation properties of Ce^{3+}-activated K_2LaCl_5, K_2LaBr_5, and K_2LaI_5 were investigated by van Loef *et al.*[48,49] These isostructural orthorhombic compounds showed high light output, up to 55 000 photons/MeV (for $K_2LaI_5:Ce^{3+}$). The iodide also showed a reasonable decay time of 24 ± 5 ns and 662 KeV energy resolution of $4.5\pm0.5\%$, although use of this scintillator is complicated because of self-activity associated with K. Our calculated structural properties are given in Table III.

$CsBa_2Br_5$ and $CsBa_2I_5$ occur in a monoclinic $P2_1/c$ (No. 14) structure.[52,53] Eu^{2+}-doped $CsBa_2I_5$ was reported to have a light yield of approximately 97 000 photons/MeV and to be less hygroscopic than $LaBr_3$ or SrI_2.[53] The calculated structural parameters are as given in Table IV.

YI_3 and BiI_3 are related materials. Ce^{3+} activated YI_3 was recently reported to have a very high light yield of almost 100 000 photons/MeV.[7,54] The related compound BiI_3 is of interest mainly as a semiconductor for radiation detection,[55] rather than as a scintillator. We include it here for comparison with YI_3. Unlike YI_3, BiI_3 has substantial covalency between Bi $6p$ and halogen p states, which leads to enhanced Born charges and may be expected to affect the optical properties.[56] These compounds occur in a rhombohedral $R\bar{3}$ structure, with the cations on site $6c(0,0,z)$ and I on $18f$ (u,v,w). With the hexagonal setting, the experimental lattice parameters are $a=7.4864$ Å, $c=20.880$ Å, for YI_3 (Ref. 57) and $a=7.516$ Å, $c=20.7180$ Å, for BiI_3 (Ref. 58). The calculated internal coordinates are $z=0.1664$, $u=0.6568$, $v=0.9993$, $w=0.4156$, for YI_3 and $z=0.1664$, $u=0.0022$, $v=0.6685$, $w=0.4123$, for BiI_3.

IV. ELECTRONIC STRUCTURE AND OPTICAL PROPERTIES

As mentioned, three functionals were used in the present study, the PBE GGA for the structural properties, and the Engel-Vosko and TB-mBJ functionals for the optical properties. The recently developed TB-mBJ has been shown to give much more accurate band gaps than other semilocal functionals in a wide variety of materials.[19] As such, we emphasize results obtained using that functional. For comparison,

the fundamental band gaps of the compounds studied are listed in Table V. The EV gaps are invariably intermediate between those of the standard PBE and the TB-mBJ functionals with the exception of the La-containing compounds. In those compounds, the f resonance is found inside the insulating gap for all three functionals. The position of the f resonance relative to the valence-band edge depends on the compound but for a given material is practically unchanged between the different functionals. For these compounds we show both the gap between the valence-band maximum and the bottom of the f bands making up the resonance, as well as the gap between the valence bands and the non-f conduction bands. Experimental band gaps are unavailable for most of these materials.

We start with BaF_2, which as mentioned is a relatively well-characterized material. The calculated band structure with the PBE, EV, and TB-mBJ functionals is as shown in Fig. 1 while the corresponding electronic density of states (DOS) is given in Fig. 2. The PBE band structure has a direct gap at Γ that is clearly underestimated with respect to

TABLE III. Structural properties of orthorhombic $Pnma$ K_2LaX_5, $X=Cl,Br,I$. The lattice parameters are from experiment (Refs. 50 and 51) while the internal parameters are from total-energy minimization using the PBE functional. The y coordinate is not listed for the atoms that are on Wyckoff site $4c$ for which $y=0.25$.

	K_2LaCl_5	K_2LaBr_5	K_2LaI_5
a (Å)	12.742	13.36	14.332
b (Å)	8.868	9.272	9.912
c (Å)	8.022	8.462	9.132
K x	0.3279	0.3277	0.3264
K y	0.9952	0.5049	0.5035
K z	0.0475	0.4465	0.4419
La x	0.0066	0.0070	0.0064
La z	0.0774	0.4202	0.4182
$X1$ x	0.1818	0.0056	0.0053
$X1$ z	0.8644	0.0646	0.0609
$X2$ x	0.0065	0.1841	0.1847
$X2$ z	0.4311	0.6329	0.6327
$X3$ x	0.2912	0.2898	0.2879
$X3$ z	0.3298	0.1674	0.1654
$X4$ x	0.0816	0.0799	0.0792
$X4$ y	0.5435	0.5459	0.5471
$X4$ z	0.1659	0.3298	0.3282

TABLE IV. Structural properties of monoclinic $P2_1/c$ CsBa$_2$X$_5$, X=Br,I. The lattice parameters are from experiment (Refs. 52 and 53) while the internal parameters are from total-energy minimization using the PBE functional.

	CsBa$_2$Br$_5$			CsBa$_2$I$_5$		
a,b,c (Å)	13.816	9.987	8.665	14.637	10.541	9.256
γ			90.2			90.194
Cs	0.1665	0.9897	0.5586	0.1675	0.9911	0.5594
Ba1	0.1768	0.5002	0.5300	0.1782	0.4999	0.5332
Ba2	0.4921	0.2511	0.5704	0.4913	0.2500	0.5772
X1	0.4211	0.9614	0.6782	0.4205	0.9562	0.6810
X2	0.0980	0.4602	0.1643	0.0956	0.4565	0.1669
X3	0.4980	0.2849	0.9535	0.4985	0.2813	0.9592
X4	0.3122	0.2868	0.3356	0.3122	0.2819	0.3375
X5	0.2192	0.2732	0.8099	0.2216	0.2694	0.8110

experiment.[59] The valence bands, of F p character, are narrow with a width of less that 2 eV, while the metal derived conduction bands are more dispersive. The EV band structure is similar to the PBE result but with a somewhat larger band gap. The mBJ band structure has a considerably enhanced gap of 9.8 eV. Furthermore, the conduction bands are distorted relative to the PBE result, with the conduction band minimum now at the X point, although it should be noted that the distinction between direct and indirect is not so important for the properties of this compound because of the very flat valence bands.

The experimental band gap of BaF$_2$ is usually quoted as 11 eV based on the measured ultraviolet reflectance spectrum.[59] This spectrum shows several features near the gap: a prominent feature at 10.00 eV, assigned as an exciton, a weaker feature at 10.57, also assigned as an exciton, and a direct band edge at 11.0 eV. Subsequent two photon absorption experiments assigned the gap as 10.6 eV.[60] The TB-mBJ direct gap at X of 9.90 eV is $\sim$1 eV lower. Importantly, the experimental spectrum has three large peaks in the valence-band region below 16 eV. The calculated TB-mBJ reflectance spectrum is shown in Fig. 3. There are two prominent peaks that can be matched with the upper two peaks in the experimental spectrum (Ref. 59) using a band shift of $\sim$1 eV. This is consistent with the assignment of the lower experimental peak as excitonic and the conclusion that the TB-mBJ band gap is underestimated by $\sim$1 eV.

The calculated refractive index is shown as a function of energy for the three functionals in Fig. 4. The refractive indices follow the trend in the band gaps with the result of the TB-mBJ functional lowest. Experimentally, the refractive index of BaF$_2$ is practically constant, rising from $n=1.465$ at low energy to $n_D=1.474$ at 589 nm (2.107 eV).[61] This is in close agreement with the results using the TB-mBJ functional. We obtain a low-frequency value of $n=1.42$ with a weak dispersion as in experiment. The low-frequency PBE value is higher at $n=1.56$ and shows a stronger energy dependence consistent with the smaller gap while the EV value of $n=1.52$ is intermediate.

This result shows that the TB-mBJ functional not only improves the band gap, but also improves the optical re-

sponse of this halide relative to the PBE functional, which is regarded as state of the art for calculations of total energies. This is important because the response depends not only on band energies but also on the wave functions, specifically through the dipole matrix elements. The charge density and total energy are fundamental quantities within densiy-

TABLE V. Calculated fundamental band gaps in electron volt for the various compounds. For La-containing compounds we list both the band gap from the valence-band edge to the La 4f resonance (denoted f) and to the conduction bands excluding the resonance (denoted cb, see text). Spin orbit is included for BiI$_3$.

	PBE	EV	TB-mBJ
BaF$_2$	6.87	7.46	9.77
BaCl$_2$	5.23	5.66	6.45
BaBr$_2$	4.45	4.85	5.39
BaIBr	3.79	4.13	4.45
BaI$_2$	3.50	3.87	4.14
CaI$_2$	3.49	3.92	4.26
SrBr$_2$	4.99	5.25	5.91
YI$_3$	2.81	3.02	3.31
BiI$_3$	1.43	1.67	1.82
Cs$_2$LiYCl$_6$	4.90	5.30	5.97
CsBa$_2$Br$_5$	4.53	5.13	5.77
CsBa$_2$I$_5$	3.69	4.14	4.49
K$_2$LaCl$_5$$f$	4.46	4.46	4.59
K$_2$LaCl$_5$ cb	5.23	5.49	6.32
K$_2$LaBr$_5$$f$	3.69	3.76	3.74
K$_2$LaBr$_5$ cb	4.33	4.66	5.26
K$_2$LaI$_5$$f$	2.79	2.95	2.80
K$_2$LaI$_5$ cb	3.38[a]	3.61	3.99
LaCl$_3$$f$	3.97	4.04	4.15
LaCl$_3$ cb	4.95	5.26	5.82
LaBr$_3$$f$	3.20	3.28	3.24
LaBr$_3$ cb	3.98	4.24	4.60

[a]f resonance overlaps bottom of conduction band.
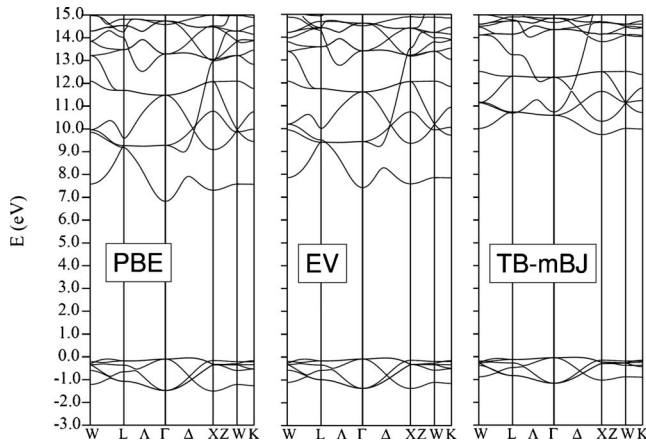
FIG. 1. Calculated band structure of BaF_2 with the three functionals.

functional theory while the single-particle energies are not. It is strongly thought that the Kohn-Sham eigenvalues of the exact density functional will not produce correct band gaps in insulators, even though its charge density and static response will be exact.[62] Therefore it is of interest to note that the improvement in the band gap of semilocal functionals, particularly going to the EV and then the TB-mBJ functional improve the static response at the same time as they improve the band gap. In the following we focus on results obtained with the TB-mBJ functional.

The calculated TB-mBJ band gap of 5.97 eV for the high light output elpasolite scintillator, Cs_2LiYCl_6 agrees well with the experimental onset of optical absorption at 5.9 eV. The refractive index is shown in Fig. 5.[41] The low-frequency limit is $n = 1.65$. There is more dispersion than in BaF_2 but the spectrum is otherwise featureless almost up to the band edge. We are not aware of experimental measurements of the optical properties of this material.

The isostructural tri-iodides, YI_3 and BiI_3 offer an interesting contrast. As mentioned, when activated with Ce^{3+}, YI_3 is a very high light output scintillator, while BiI_3 is not. The emission of $YI_3:Ce^{3+}$ starts at ∼2.9 eV and peaks at 2.26 eV.[7] The high-energy onset is below our calculated TB-mBJ gap of 3.31 eV but is higher than the gap obtained with the standard PBE GGA and prior calculations done with the local-density approximation.[63] The difference between YI_3 and BiI_3 can be understood in terms of the electronic struc-
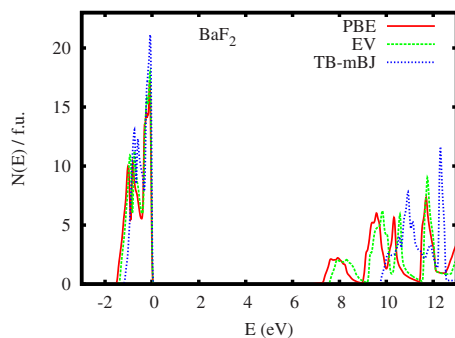
FIG. 2. (Color online) Electronic density of states of BaF_2 as calculated with the PBE, EV, and TB-mBJ functionals.
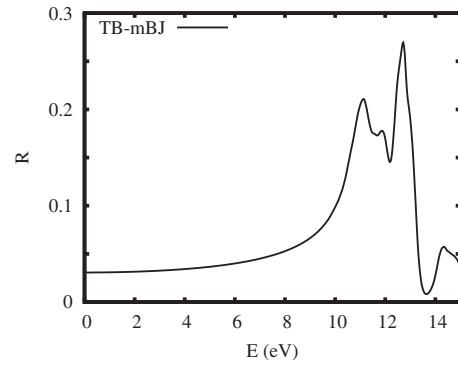
FIG. 3. Calculated TB-mBJ reflectivity spectrum of BaF_2.

ture, specifically that the band gap of BiI_3 is too small and that this is due to low-lying Bi $6p$ states.

In order for scintillation to take place an electron-hole pair must recombine at the Ce^{3+} site. For this to be efficient both the upper and lower states for the activator ion should be in the band gap. This is evidently not possible in BiI_3. As mentioned, the Ce^{3+} emission in YI_3 has a high-energy onset of 2.9 eV, which is similar to that in other iodides. This is a lower bound on the energy difference between the upper and lower states of the activator ion. A comparison of the calculated TB-mBJ electronic DOS of the two materials is given in Fig. 6. The lowest conduction bands in YI_3 are formed from Y $4d$ states. In contrast, there is a manifold of Bi $6p$ states making up the conduction bands in BiI_3, and these occur at lower energy. This leads to a 1.49 eV lower band gap in the Bi compound. Our TB-mBJ gap for BiI_3 is substantially higher than that obtained in prior calculations using other functionals[64,65] but it is still only 1.82 eV. The experimental optical gap is 2.0 eV.[66] This does not leave a sufficient energy range for both the upper and lower states to be in the gap. This is similar to the problem in activating Pb phosphate glasses with rare earths.[67] In fact, considering the fact that, all things being equal, lower gaps favor higher light output, but that too low a gap prevents activation, the gap of YI_3 is probably close to optimum for a Ce^{3+}-activated material.

The refractive indices of YI_3 and BiI_3 are presented in Fig. 7. Surprisingly, the refractive index of YI_3 is almost isotropic, even though the material itself is structurally very anisotropic as shown in Fig. 8. The low-energy limits of the
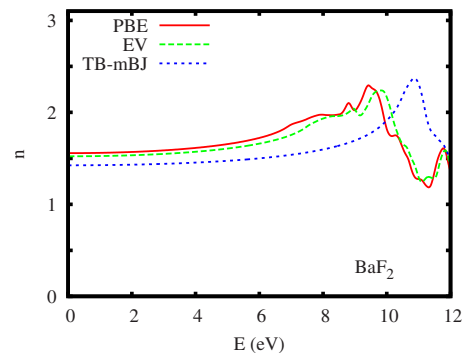
FIG. 4. (Color online) Calculated refractive index of BaF_2 with the three functionals.
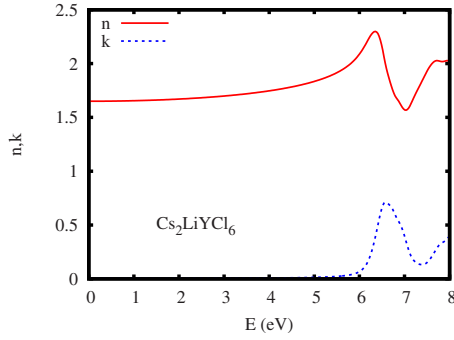
FIG. 5. (Color online) Calculated refractive index of Cs_2LiYCl_6.

refractive indices of YI_3 are $n_{xx}=2.08$ and $n_{zz}=2.06$, which is an anisotropy of 1%. BiI_3 is slightly less isotropic but is still remarkably so for such an anisotropic layered crystal structure. The low-energy refractive indices are $n_{xx}=2.76$ and $n_{zz}=2.71$ for BiI_3. Jellison *et al.*[66] reported a value of 3.1 at 1.6 eV. For comparison, our calculated values at 1.6 eV are 3.16 in plane (xx) and 3.02 out of plane (zz), in excellent agreement with the experiment.

We find a similar remarkable near isotropy of the optical properties in several other halides as well. This is the case even for monoclinic $CsBa_2Br_5$ and $CsBa_2I_5$ as shown in Fig. 9. The three diagonal components of the refractive index are practically the same almost up to the band edge while the off-diagonal component associated with the monoclinic symmetry is practically zero over this energy range.

For comparison, we also performed calculations for monoclinic $CdWO_4$. We followed the same procedure relaxing the internal coordinates using the PBE functional and then performing optical calculations using the TB-mBJ functional. The calculated band gaps are 2.99 eV with the PBE functional and 4.16 eV with the TB-mBJ form. The PBE value is similar to that obtained previously by Abraham *et al.*[68] The TB-mBJ value is close to the experimental value of 3.8–4.1 eV (see Ref. 68). The refractive index is shown in Fig. 10. As may be seen, in contrast to the halides, it is quite anisotropic with a substantial off-diagonal component.

Returning to halides, we next discuss La-containing materials. The band structure of these materials may be described as that of an equivalent material based on a simple trivalent ion, e.g., Y, plus additional unoccupied f derived
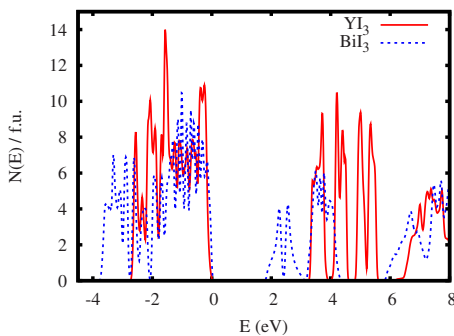
FIG. 6. (Color online) Comparison of the electronic DOS of YI_3 and Bi_3 as obtained with the TB-mBJ functional.
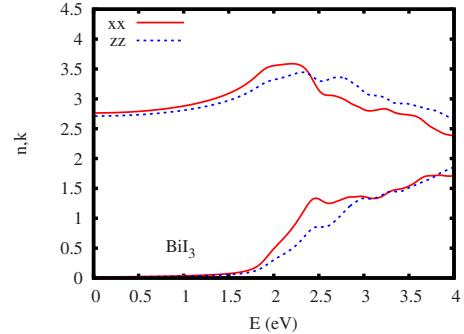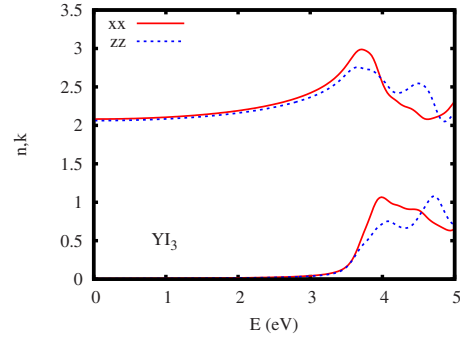
FIG. 7. (Color online) Calculated refraction of YI_3 (top) and BiI_3 (bottom) as a function of energy based on the TB-mBJ functional. The upper set of curves are n and the lower set are k.

bands that occur in the band gap. The f bands comprise the so-called f resonance. In Table V we give both the value of the fundamental gap, which is from the top of the halogen p derived valence bands to the bottom of the f resonance as well as a larger gap, denoted "cb," which is from the top of the valence bands to the bottom of the conduction bands, excluding the f resonance.

We find that in contrast to the band gaps of the other materials studied, the fundamental gap of these materials is practically unchanged upon going from the PBE to the TB-
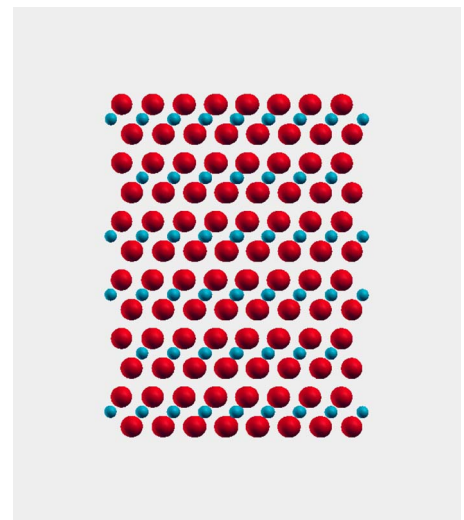
FIG. 8. (Color online) Crystal structure of YI_3 with the relaxed atomic positions. The large red balls denote I while the smaller gray balls are Y. Note the layered structure.
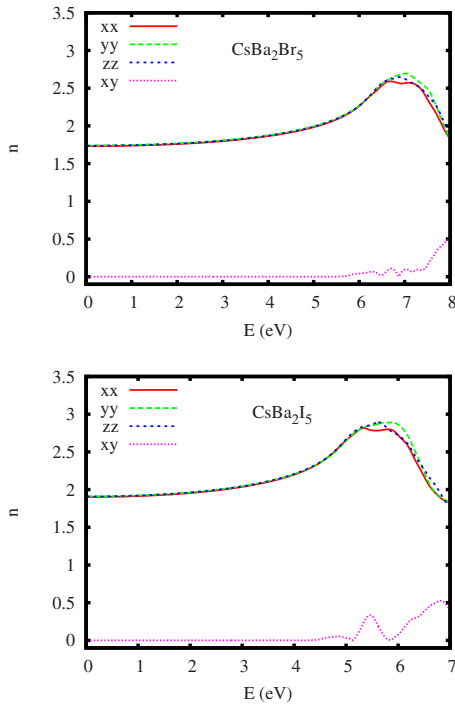
FIG. 9. (Color online) Calculated refraction for $CsBa_2Br_5$ (top) and $CsBa_2I_5$ (bottom) based on the TB-mBJ functional.

mBJ functional. That is the position of the f bands relative to the valence-band maximum is almost the same with these three functionals. This is illustrated for $LaBr_3$ and K_2LaBr_5 in Fig. 11. The position of the higher lying non-f conduction bands is, however, increased with the TB-mBJ functional. This does lower the optical refractive index, even though the fundamental band gap is unchanged.

The calculated refractive indices of $LaCl_3$ and $LaBr_3$ are shown in Fig. 12. The low-energy values are $n_{xx}=1.87$ and $n_{zz}=1.91$ for $LaCl_3$ and $n_{xx}=2.04$ and $n_{zz}=2.09$ for $LaBr_3$. This follows the expected trend where bromides have higher refractive index than chlorides. Again, we find low anisotropy in materials that are structurally anisotropic. The same trend with halogen atomic number and also very low optical anisotropy is found in K_2LaCl_5, K_2LaBr_5, and K_2LaI_5, as shown in Fig. 13. The calculated TB-mBJ band gap to the non-f upper conduction-band edges (cb) for K_2LaCl_5, K_2LaBr_5, and K_2LaI_5 are 6.32 eV, 5.26 eV, and 3.99 eV,
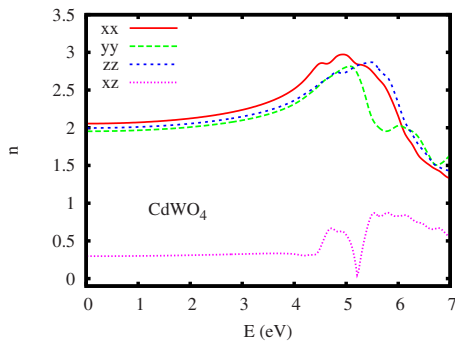
FIG. 10. (Color online) Calculated refraction for $CdWO_4$ with the TB-mBJ functional.
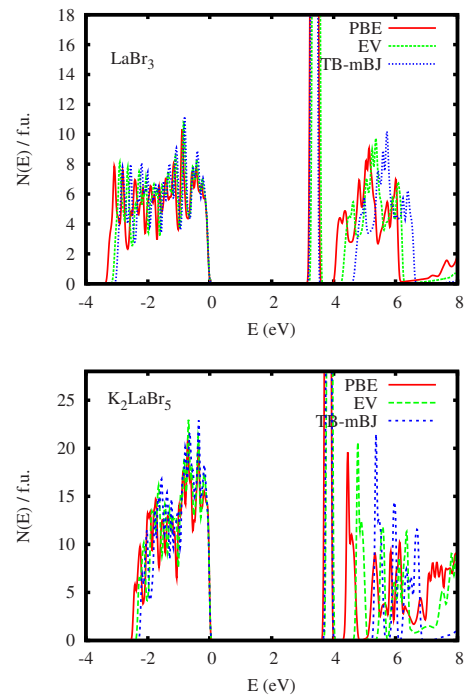
FIG. 11. (Color online) Comparison of the DOS with the three functionals for $LaBr_3$ (top) and K_2LaBr_5 (bottom). Note that the position of the f resonance that sets the fundamental gap is relatively unaffected by the changes in functional.

respectively, as compared to the experimental estimates of 6.6 eV, 5.5 eV, and 4.5 eV.[48,49]

The refractive indices of $BaCl_2$, $BaBr_2$, $BaIBr$, and BaI_2 are given in Fig. 14 while those of CaI_2 and $SrBr_2$ are given
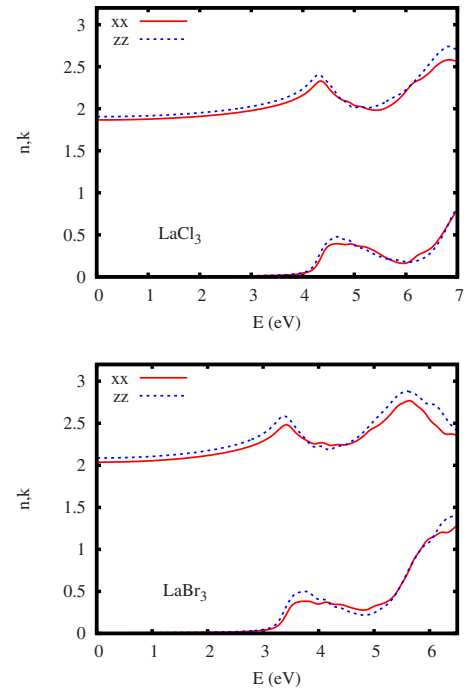
FIG. 12. (Color online) Calculated refraction for $LaCl_3$ (top) and $LaBr_3$ (bottom) based on the TB-mBJ functional. The upper set of curves are n and the lower set are k.
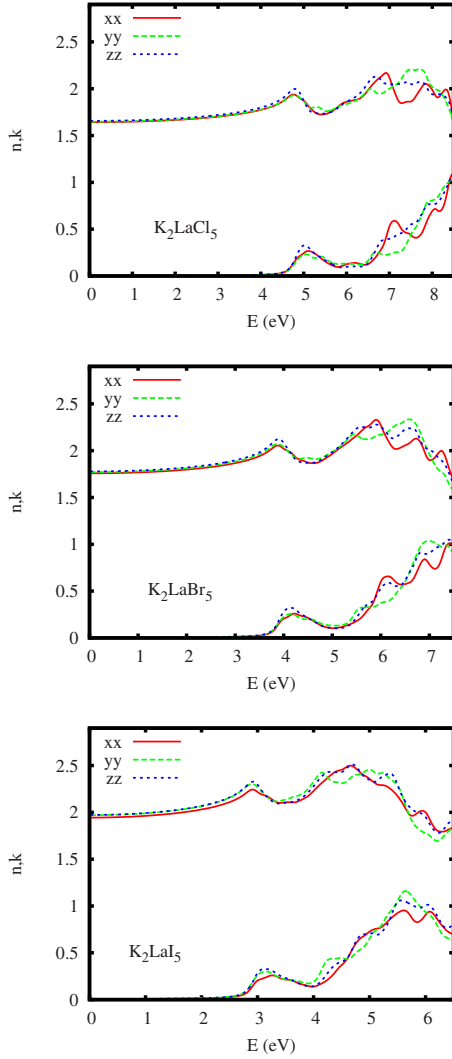
FIG. 13. (Color online) Calculated refraction for K_2LaCl_5 (top), K_2LaBr_5 (middle), and K_2LaI_5 (bottom) based on the TB-mBJ functional. The upper set of curves are n and the lower set are k.

in Figs. 15 and 16, respectively. The calculated TB-mBJ band gap for $BaCl_2$ of 6.45 eV is in reasonable accord with the estimate from Cl K x-ray spectroscopy of 7.0 eV.[69] As mentioned, $BaCl_2$, $BaBr_2$, $BaIBr$, and BaI_2 occur in a complex orthorhombic *Pnma* structure. $SrBr_2$ is tetragonal while CaI_2 is rhombohedral. None of these materials is cubic. CaI_2 activated with Eu^{2+} has been known to be an extremely high light output material since the 1960s.[26] However, this hexagonal material has not been used in applications because of crystal growth problems due to its platelet growth habit. Nonetheless, again we find only very small anisotropy in the optical properties for all of these materials, similar to what we found previously for SrI_2.[10]

V. DISCUSSION

We have two main conclusions, besides the numerical data, which we hope will be useful in improving the design of scintillator systems for better light coupling. First of all, we find that the newly developed TB-mBJ functional greatly
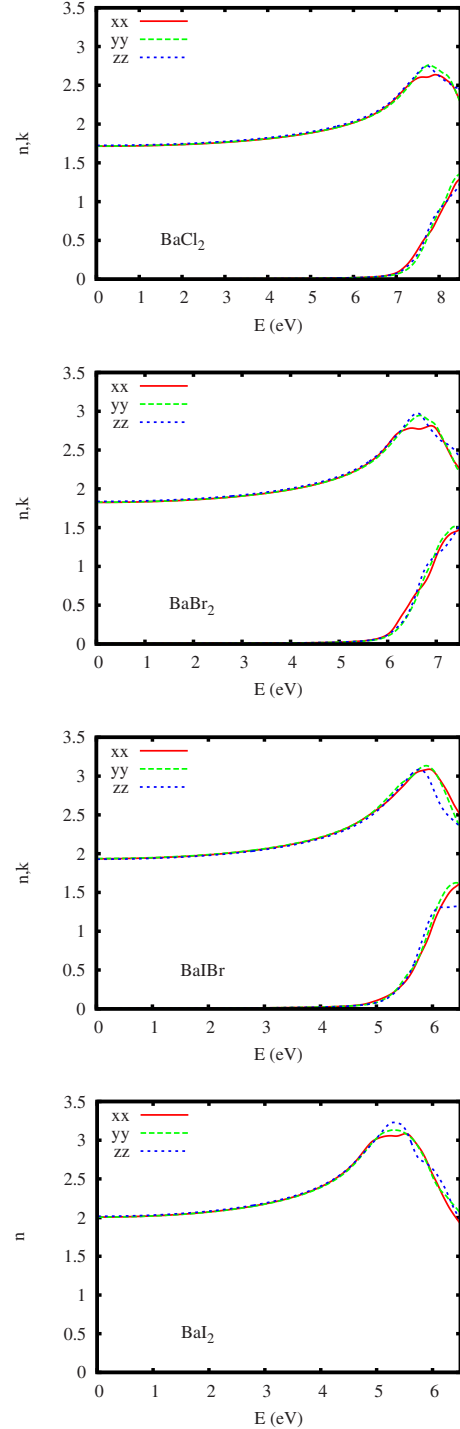
FIG. 14. (Color online) Calculated refraction for $BaCl_2$, $BaBr_2$, $BaIBr$, and BaI_2, from top to bottom using the TB-mBJ functional. The upper set of curves are n and the lower set are k.

improves both the band gaps and the optical properties in a broad class of halide materials, consistent with results reported for other compounds.[19] Considering the computational efficiency of this method, which is similar to standard density-functional methods, we expect that this method will enable optical characterization of new complex halide scintillators and perhaps, considering that band gap is a key pa-
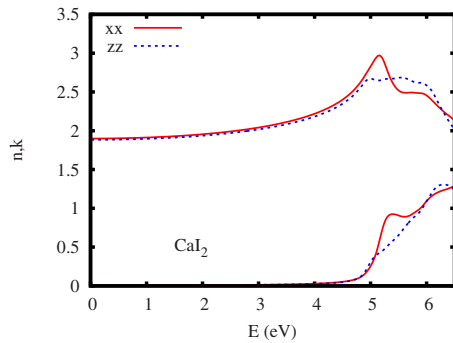
FIG. 15. (Color online) Calculated refraction for CaI_2 based on the TB-mBJ functional. The upper set of curves are n and the lower set are k.

FIG. 16. (Color online) Calculated refraction for $SrBr_2$ based on the TB-mBJ functional. The upper set of curves are n and the lower set are k.

rameter, more effective theoretical screens for new scintillators.

Second, and quite unexpectedly, we find that a wide variety of halide scintillators based on Cl, Br, and I are practically isotropic from an optical point of view, even though many of them are highly anisotropic from the point of view of structure and other properties. The broad range of materials in which this occurs implies that it is a general feature of halide chemistry rather than a special coincidence for certain compounds.

Qualitatively, it may be understood from the coordination environments and general band structure features. In particular, these materials have relatively wide band gaps due to the large electronegativity difference between the cations and the halogen atoms. The halogen p derived valence bands are narrow compared to typical metal oxides. This narrow bandwidth suggests that one can understand the properties in real space instead of depending essentially on detailed band dispersions. Additionally, the valence-band formation comes at least largely from direct hoping between the halogen p orbitals on adjacent sites these materials. The structures can be described in anion contact terms.[2] From a structural point of view, the anion lattices of these compounds are distortions of high symmetry structures with most of the anisotropy coming from the cation placement in the intertices of the anion lattice. This places the cations in locally highly symmetric cages based on high nearest-neighbor anion coordination numbers. Since the anion bands are relatively nondispersive, the main crystal structure dependence comes from the con-

duction bands. Therefore, the small optical anisotropy of these materials can be rationalized in terms of the highly symmetric local environments of the cations as far as nearest-neighbor anion coordination is concerned. Further work to elucidate this is clearly needed.

In any case, this result has important implications for the development of halide scintillators. Gamma spectroscopy requires high-quality uniform crystals of sufficient size to effectively stop the gamma rays in the scintillator volume. This typically requires cm sized crystals and many applications benefit from still larger sizes. As a result, crystal growth is one of the main challenges in the development of new halide scintillators. The near optical isotropy of these materials, however, suggests that ceramic scintillators of sufficient size to be useful for gamma spectroscopy can be made. While this will require solution of a number of problems, for example, the development of methods to produce dense sintered bodies without contamination in these often hygroscopic, air sensitive materials, it may enable the use of low symmetry difficult to grow halide materials for gamma spectroscopy and other scintillator applications. Furthermore, ceramic materials are generally lower cost than single crystals, especially if large volumes of material are needed.

[1] G. Knoll, *Radiation Detection and Measurement*, 3rd ed. (Wiley, New York, 2000).

[2] L. Pauling, *The Nature of the Chemical Bond and the Structure of Molecules and Crystals: An Introduction to Modern Structural Chemistry*, 3rd ed. (Cornell University Press, Ithaca, N.Y., 1960).

[3] G. Meyer, Prog. Solid State Chem. **14**, 141 (1982).

[4] J. T. M. de Haas and P. Dorenbos, IEEE Trans. Nucl. Sci. **55**, 1086 (2008).

[5] E. V. D. van Loef, P. Dorenbos, C. W. E. van Eijk, K. Kramer,

and H. U. Gudel, Appl. Phys. Lett. **79**, 1573 (2001).

[6] N. J. Cherepy *et al.*, Appl. Phys. Lett. **92**, 083508 (2008).

[7] J. Glodo, E. V. D. van Loef, W. M. Higgins, and K. S. Shah, IEEE Trans. Nucl. Sci. **55**, 1496 (2008).

[8] A. Lempicki, C. Brecher, H. Lingertat, and V. K. Sarin, U.S. Patent No. 6,967,330 (22 November 2000).

[9] D. J. Wisniewski *et al.*, IEEE Trans. Nucl. Sci. **55**, 1501 (2008).

[10] D. J. Singh, Appl. Phys. Lett. **92**, 201908 (2008).

[11] P. Blaha, K. Schwarz, G. Madsen, D. Kvasnicka, and J. Luitz, in *WIEN2k: An Augmented Plane Wave+Local Orbitals Program*

for Calculating Crystal Properties, edited by K. Schwarz (Technische Universität Wien, Austria, 2001).

[12] D. Singh, Phys. Rev. B **43**, 6388 (1991).

[13] J. P. Perdew, K. Burke, and M. Ernzerhof, Phys. Rev. Lett. **77**, 3865 (1996).

[14] J. P. Perdew, J. A. Chevary, S. H. Vosko, K. A. Jackson, M. R. Pederson, D. J. Singh, and C. Fiolhais, Phys. Rev. B **46**, 6671 (1992).

[15] E. Engel and S. H. Vosko, Phys. Rev. B **47**, 13164 (1993).

[16] P. Dufek, P. Blaha, and K. Schwarz, Phys. Rev. B **50**, 7279 (1994).

[17] D. J. Singh, Phys. Rev. B **81**, 195217 (2010).

[18] G. E. Jellison, Jr., S. Auluck, D. J. Singh, and L. A. Boatner, J. Appl. Phys. **107**, 013514 (2010).

[19] F. Tran and P. Blaha, Phys. Rev. Lett. **102**, 226401 (2009).

[20] M. Laval, M. Mosszynski, R. Allemand, E. Cormoreche, P. Guinet, R. Odru, and J. Vacher, Nucl. Instrum. Methods Phys. Res. **206**, 169 (1983).

[21] C. L. Woody, P. W. Levy, and J. A. Kierstead, IEEE Trans. Nucl. Sci. **36**, 536 (1989).

[22] R. Visser, P. Dorenbos, C. W. E. van Eijk, R. W. Hollander, and P. Schotanus, IEEE Trans. Nucl. Sci. **38**, 178 (1991).

[23] A. J. Wojtowicz, P. Szupryczynski, J. Glodo, W. Drozdowski, and D. Wisniewski, J. Phys.: Condens. Matter **12**, 4097 (2000).

[24] L. E. Dinca, P. Dorenbos, J. T. M. de Haas, V. R. Bom, and C. W. E. Van Eijk, Nucl. Instrum. Methods Phys. Res. A **486**, 141 (2002).

[25] A. H. Swanson and E. Tatge, *Standard X-ray Diffraction Powder Patterns*, Natl. Bur. Stand. Ref. Data Ser., Natl. Bur. Stand. (U.S.), Circ. No. 539 (U.S. GPO, Washington, DC, 1953).

[26] R. Hofstadter, E. W. O'Dell, and C. T. Schmidt, IEEE Trans. Nucl. Sci. **11**, 12 (1964).

[27] R. Hofstadter, E. W. O'Dell, and C. T. Schmidt, Rev. Sci. Instrum. **35**, 246 (1964).

[28] A. Jestin Lenus, D. Sornadurai, K. Govinda Rajan, and B. Purniah, Mater. Lett. **57**, 635 (2002).

[29] J. Selling, M. D. Birowosuto, P. Dorenbos, and S. Schweizer, J. Appl. Phys. **101**, 034901 (2007).

[30] J. Selling, S. Schweizer, M. D. Birowosuto, and P. Dorenbos, J. Appl. Phys. **102**, 074915 (2007).

[31] M. Koshimizu, K. Onodera, K. Shibuya, H. Saito, and K. Asai, J. Appl. Phys. **105**, 114912 (2009).

[32] E. D. Bourret-Courchesne, G. Bizarri, S. M. Hanrahan, G. Gundiah, Z. Yan, and S. E. Derenzo, Nucl. Instrum. Methods Phys. Res. A **613**, 95 (2010).

[33] K. Shal, Heidelb. Beitr. Mineral. Petrogr. **9**, 111 (1963).

[34] W. Döll and W. Klemm, Z. Anorg. Allg. Chem. **241**, 239 (1939).

[35] B. Frit, M. Mokail-Chbany, and P. Hagenmuller, C. R. Seances Acad. Sci., Ser. C **267**, 1046 (1968).

[36] J. G. Smeggil and H. A. Eick, Inorg. Chem. **10**, 1458 (1971).

[37] H. Blum, Z. Phys. Chem. Abt. B **22**, 298 (1933).

[38] B. Morosin, J. Chem. Phys. **49**, 3007 (1968).

[39] K. Krämer, T. Schleid, M. Schulze, W. Urland, and G. Meyer, Z. Anorg. Allg. Chem. **575**, 61 (1989).

[40] C. W. E. van Eijk, J. T. M. de Haas, P. Dorenbos, K. W. Kramer, and H. U. Gudel, IEEE Nuclear Science Symposium Conference Record, 2005 (IEEE), Vol. 1, p. 239.

[41] E. V. D. van Loef, P. Dorenbos, C. W. E. van Eijk, K. W. Kramer, and H. U. Gudel, J. Phys.: Condens. Matter **14**, 8481 (2002).

[42] M. D. Birowosuto, P. Dorenbos, C. W. E. van Eijk, K. W. Kramer, and H. U. Gudel, J. Phys.: Condens. Matter **18**, 6133 (2006).

[43] M. D. Birowosuto, P. Dorenbos, J. T. M. de Haas, C. W. E. van Eijk, K. W. Kramer, and H. U. Gudel, IEEE Trans. Nucl. Sci. **55**, 1152 (2008).

[44] A. Bessière, P. Dorenbos, C. W. E. van Eijk, L. Pidol, K. W. Krämer, and H. U. Güdel, J. Phys.: Condens. Matter **16**, 1887 (2004).

[45] J. Grimm, J. Fleniken, K. W. Kramer, D. Biner, U. Happek, and H. U. Gudel, J. Lumin. **122-123**, 325 (2007).

[46] W. M. Higgins, J. Glodo, U. Shirwadkar, A. Churilov, E. Van Loef, R. Hawrami, G. Ciampi, C. Hines, and K. S. Shah, J. Cryst. Growth **312**, 1216 (2010).

[47] C. Reber, H. U. Guedel, G. Meyer, T. Schleid, and C. A. Daul, Inorg. Chem. **28**, 3249 (1989).

[48] E. V. D. van Loef, P. Dorenbos, C. W. E. van Eijk, K. W. Kramer, and H. U. Gudel, Phys. Rev. B **68**, 045108 (2003).

[49] E. V. D. van Loef, P. Dorenbos, C. W. E. van Eijk, K. W. Kramer, and H. U. Güdel, Nucl. Instrum. Methods Phys. Res. A **537**, 232 (2005).

[50] G. Meyer and E. Huttl, Z. Anorg. Allg. Chem. **497**, 191 (1983).

[51] G. Meyer, J. Soose, A. Moritz, V. Vitt, and T. Hollhes, Z. Anorg. Allg. Chem. **521**, 161 (1985).

[52] G. Schilling and G. Meyer, Z. Kristallogr. **211**, 255 (1996).

[53] E. D. Bourret-Courchesne, G. Bizarri, R. Borade, Z. Yan, S. M. Hanrahan, G. Gundiah, A. Chaudhry, A. Canning, and S. E. Derenzo, Nucl. Instrum. Methods Phys. Res. A **612**, 138 (2009).

[54] E. V. van Loef, W. M. Higgins, J. Glodo, A. V. Churilov, and K. S. Shah, J. Cryst. Growth **310**, 2090 (2008).

[55] D. Nason and L. Keller, J. Cryst. Growth **156**, 221 (1995).

[56] M. H. Du and D. J. Singh, Phys. Rev. B **82**, 045203 (2010).

[57] L. Jongen and G. Meyer, Acta Crystallogr., Sect. E: Struct. Rep. Online **61**, i51 (2005).

[58] J. Trotter and T. Zobel, Skr. Nor. Vidensk.-Akad., [Kl.] 1: Mat.-Naturvidensk. Kl. **1947**, 73 (1947).

[59] G. W. Rubloff, Phys. Rev. B **5**, 662 (1972).

[60] T. Tsujibayashi, K. Toyoda, S. Sakuragi, M. Kamada, and M. Itoh, Appl. Phys. Lett. **80**, 2883 (2002).

[61] R. D. Shannon, R. C. Shannon, O. Medenbach, and R. X. Fischer, J. Phys. Chem. Ref. Data **31**, 931 (2002).

[62] R. O. Jones and O. Gunnarson, Rev. Mod. Phys. **61**, 689 (1989).

[63] R. Boutchko, A. Canning, A. Chaudhry, R. Borade, E. Bourret-Courchesne, and S. E. Derenzo, IEEE Trans. Nucl. Sci. **56**, 977 (2009).

[64] M. Schlüter, M. L. Cohen, S. E. Kohn, and C. Y. Fong, Phys. Status Solidi B **78**, 737 (1976).

[65] H. Yorikawa and S. Muramatsu, J. Phys.: Condens. Matter **20**, 325220 (2008).

[66] G. E. Jellison, Jr., J. O. Ramey, and L. A. Boatner, Phys. Rev. B **59**, 9718 (1999).

[67] D. J. Singh, G. E. Jellison, Jr., and L. A. Boatner, Phys. Rev. B **74**, 155126 (2006).

[68] Y. Abraham, N. A. W. Holzwarth, and R. T. Williams, Phys. Rev. B **62**, 1733 (2000).

[69] C. Sugiura, Phys. Rev. B **9**, 2679 (1974).